MIT Libraries | DSpace@MIT

MIT Open Access Articles

Terahertz tomography using quantum-cascade lasers

The MIT Faculty has made this article openly available. ***Please share*** how this access benefits you. Your story matters.

Massachusetts Institute of Technology

Terahertz tomography using quantum-cascade lasers

Alan Wei Min Lee[1,2,*], Tsung-Yu Kao[1], David Burghoff[1], Qing Hu[1], and John L. Reno[3]

[1]*Massachusetts Institute of Technology, Cambridge, Massachusetts 02139, USA*

[2]*LongWave Photonics LLC, Boston, Massachusetts 02129, USA*

[3]*Center for Integrated Nanotechnologies, Sandia National Laboratories, Albuquerque, New Mexico 87185–0601, USA*

*Corresponding author: awmlee@longwavephotonics.com

The interfaces of a dielectric sample are resolved in reflection geometry using light from a frequency agile array of terahertz quantum-cascade lasers. The terahertz source is a 10-element linear array of third-order distributed-feedback QCLs emitting at discrete frequencies from 2.08 to 2.4 THz. Emission from the array is collimated and sent through a Michelson interferometer, with the sample placed in one of the arms. Interference signals collected at each frequency are used to reconstruct an interferogram and detect the interfaces in the sample. Because of the long coherence length of the source, the interferometer arms need not be adjusted to the zero-path delay. A depth resolution of 360 μm in the dielectric is achieved with further potential improvement through improved frequency coverage of the array. The entire experiment footprint is <1 m × 1 m with the source operated in a compact, closed-cycle cryocooler.   © 2012 Optical Society of America

OCIS codes: 140.3070, 140.0140.

Tomography of dielectric thin films using terahertz-frequency radiation (300 GHz to 10 THz) has found recent practical applications for the characterization of industrial polymers [1–3]. The opacity of these polymers at the near-IR and visible frequencies precludes the use of more mature technologies, justifying the expense and complexity of the nonlinear generation mechanisms of current commercial terahertz systems. As an alternative, quantum-cascade lasers (QCLs) are a promising fundamental source of terahertz frequency radiation for their multimilliwatt power levels, electrical operation, and absence of optical alignment. However, the use of QCLs for the tomography of dielectric films is challenging due to the lack of picosecond pulsed sources necessary for time-of-flight tomography or the practical frequency tuning mechanisms necessary for interferometry-based tomography. In this Letter we report a frequency agile QCL source and the demonstration of tomography using the swept-source optical coherence tomography (SS-OCT) technique [4–5]. Here a Michelson interferometer is used with the frequency agile source in order to reconstruct an interferogram resulting from the reflections from the interfaces of a sample and the reflections from a movable reference mirror. Peaks in the interferogram indicate the presence of discontinuities in the sample, allowing depth measurement.

A frequency agile source was developed for this work [Fig. 1(a)], which is a 21-element linear array of third-order distributed feedback (DFB) QCLs following those demonstrated in [6–7]. The third-order DFB consists of a metal–metal waveguide, which provides confinement of the optical mode, combined with lateral corrugations for frequency-selective feedback. The $\sim\lambda_o/2$ spacing of the corrugations, along with the alternating phase of the field, results in coherent addition along the ridge leading to the narrow, symmetric beam patterns. Each element in the array is designed to emit at a slightly different frequency, similar to the first-order DFB QCL arrays demonstrated at mid-IR frequencies in [8]. This approach has several advantages over mechanical tuning mechanisms: it is mechanically robust because it does not have moving

parts; and the frequency switching speed is only limited by the drive electronics and the device parasitics.

The third-order DFB array was fabricated using standard metal–metal waveguide fabrication techniques, using contact lithography and electron cyclotron resonance–reactive ion etching to define the laser mesas using the Ti/Au top contact as the self-aligned etch mask. An additional SiO_2 electrical insulation layer was used for the isolation of the contact pads. The active region of the array (FL175M-M3, MBE wafer EA1222) is based on the resonant-phonon depopulation design lasing primarily around 2.2 THz in a Fabry–Perot metal–metal waveguide, and was previously characterized in [9]. Each element in
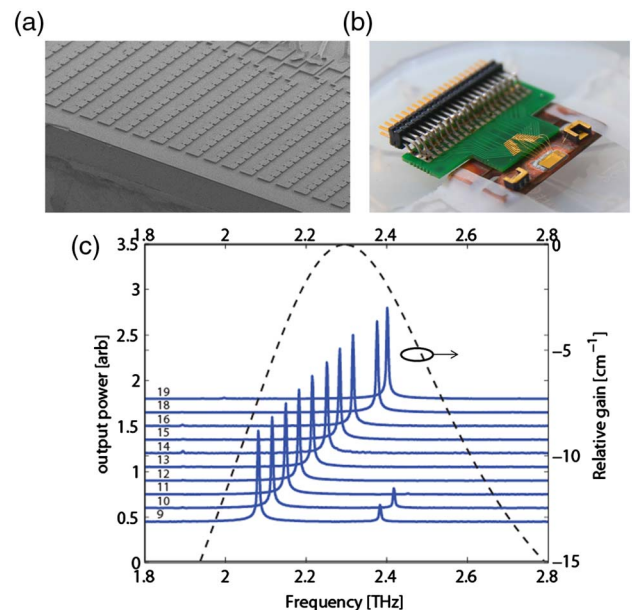

Fig. 1.   (Color online) (a) SEM of 21-element third-order DFB grating QCL array with system packaged in (b). (c) Spectra of QCLs in an array (devices numbered at left) showing frequency separation $\sim$40 GHz. Devices 9 through 19 show frequency coverage of 320 GHz. Dashed line indicates fit to the measured gain of the QCL active region from [9].

© 2012 Optical Society of America

the array was designed to have a frequency separation of ~40 GHz, spanning a frequency range of 1.8 to 2.6 THz (grating periods ranging from 54 to 77 μm). Devices have a width of 40 μm and a variable number of grating periods to keep the overall device length to close to 1 mm, irrespective of the grating period.

Several individual QCLs were lost during the wire bonding process, due to the relatively small (150 μm pitch) bonding pads. The remaining devices were tested in pulsed mode (500 ns at ~10% duty cycle) at 48 K, with the resulting spectra measured by Fourier transform IR spectroscopy shown in Fig. 1(b). Devices 9 through 19 were observed to lase primarily in their intended modes, spanning a frequency range of 2.08 to 2.4 THz. This frequency range effectively exhausts the gain spectrum of this active region, which is plotted in Fig. 1b from [9].

The frequency coverage for the 10 devices from 9 to 19 is 320 GHz and is sufficient for a proof-of-concept SS-OCT system. Peak optical power was measured using a thermopile power meter (ScienTech AC2500H) with the highest peak level obtained, ~1.5 mW, for device 16—which has a lasing frequency near the center of the gain spectrum. Threshold current densities ranged from 290 A/cm^2 to 340 A/cm^2 with no obvious trend across all devices.

The QCL array was mounted in a closed cycle, Stirling cycle cryocooler weighing less than <12 kg and with a footprint of 32 cm × 38 cm (Ricor K535). The source was integrated in the SS-OCT setup shown in Fig. 2. The beams emitted from the array are collimated by an $f/1$ silicon lens and split into two arms by a quartz beam splitter. The reference arm has a movable mirror, while the sample arm is fixed. The recombined light is focused using an $f/1$ silicon lens onto a Ga:Ge photodetector. Computer-controlled biasing electronics were built, allowing for software addressing of up to 16 devices. A field-programmable gate array (FPGA) is used

to generate timing signals to synchronously bias the laser and trigger a lock-in amplifier for detection. The FPGA also generates control signals for a variable power supply and multiplexer control signals, allowing for rapid change of the output frequency. Software developed to control the QCL biasing allows <10 ms cycling of devices. Even faster switching times of <10 μs are possible by programming the switching into the FPGA directly.

Interferometric measurements were taken in pulsed mode (500 ns pulse width, 7% duty cycle), with either a mirror in the sample arm (for normalization) or a sample of 380 μm thick polypropylene in front of the sample mirror. In either case, the reference was stepped 30 times over a total distance of 140 μm. At each step, the signal was acquired for each of the lasers via a lock-in amplifier at the pulse repetition rate. The interference patterns are shown ("+" symbols) for a few different devices without a sample [Fig. 3(a)] and with the 380 μm thick sample [Fig. 3(b)]. The sinusoidal modulations are apparent even at large path differences between the reference and sample arms of the interferometer, due to the long coherence length of the QCL source. It should be pointed out that
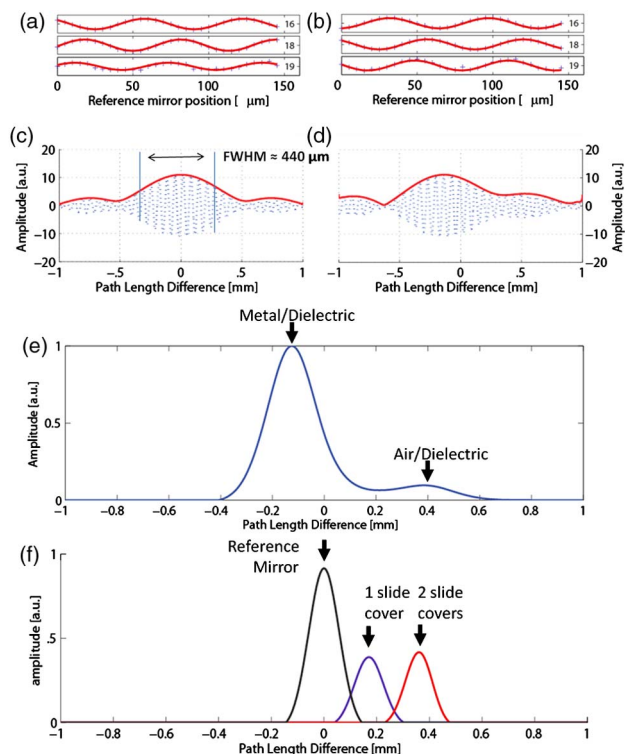
Fig. 3. (Color online) (a), (b) Interference signals (blue "+") and numerical fit (red line) for various devices as a function of position of the reference mirror without (a) and with (b) a 380 μm thick sample, respectively. (c), (d) Reconstructed interferogram (blue dashed trace, envelope as red solid trace) without and with the sample, respectively. (e) Numerically sharpened version of (d) using deconvolution. Arrows indicate strong reflection at the mirror/dielectric interface and a weaker reflection at the dielectric/air interface. (f) Three numerically sharpened measurements: reference mirror, reference mirror + 180 μm thick glass slide cover, and reference mirror + two glass slide covers. The strong front (glass/air) reflection clearly indicates the thickness of the sample. A weak metal/glass interface does not appear due to the absorption of the glass.
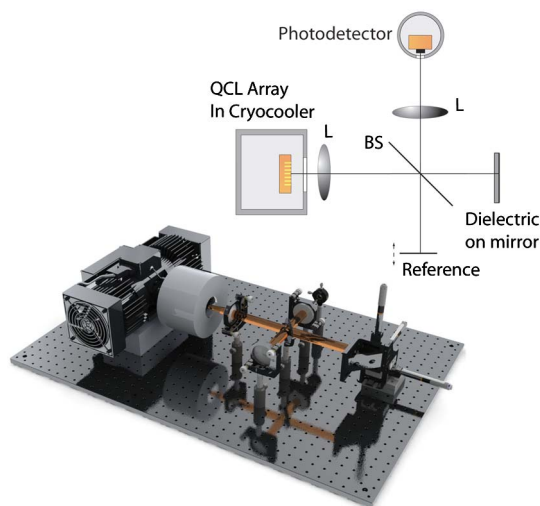

Fig. 2. (Color online) Illustration of the SS-OCT system (schematic above). Components: frequency agile QCL array inside the compact cryocooler; lens (L) collimating the beam through the Michelson interferometer consisting of a beam splitter (BS), reference arm (REF), and sample arm. A polypropylene test sample is shown, with reflections occurring at the air/polypropylene and polypropylene/metal interfaces.

this is a key advantage of this approach over time-domain approaches, as the zero-path delay need not be found, simplifying the interferometer setup.

After the interference signal is acquired, a numerical fit is used to determine the amplitude, period, and phase of the modulation (continuous red traces). Amplitude normalization is performed, and the interference signals are summed, resulting in the (blue dashed) interferogram shown in Fig. 3(c) without the sample. Figure. 3(d) shows the interferogram and its envelope when the sample is present, clearly showing a shift in the position of the peak. To increase the apparent resolution, numerical enhancement via deconvolution is performed. Here the reference signal [Fig. 3(c)] is deconvolved from the measured signal [Fig. 3(d)] using the Richardson–Lucy algorithm for $N = 20$ iterations resulting in the trace in part (e) [10]. The position of the air/polypropylene interface occurs at ~380 μm because the sample arm is shortened by insertion of the sample (i.e., the first interface is closer to the beam splitter). The polypropylene/metal interface appears at ~ -160 μm for a total *apparent* thickness of 540 μm. The apparent thickness and the actual thickness can be used to calculate the mean index of refraction of the sample, $n_{\mathrm{poly}} = 540$ μm/380 μm = 1.42. Additional characterization of the thickness measurements were done on 180 μm thick glass slides [Fig. 3(f)]. In this case, only the glass/air interface is resolvable due to the strong attenuation in the glass.

The FWHM depth resolution (Δz) is given by the bandwidth of the source approximately as $\Delta z = c/2 \cdot n \cdot \Delta f$, where c is the speed of light, n is the index of refraction of the sample, and Δf is the bandwidth of the source in hertz. For the present system, this limits the depth resolution to approximately 360 μm in polypropylene or 470 μm in air, which is close to the measured FWHM of 440 μm in Fig. 3(c). A finer depth resolution can be achieved by using an active region with a broader spectral gain for broader tuning [11].

The acquisition time of this experiment was ~40 s, discounting the ~5 s required for the lock-in amplifier to reacquire a phase lock when a laser is switched. The primary limitation on the acquisition speed is the large number (30) of reference mirror scan steps used to determine the amplitude and phase of the interference signals of Figs. 3(a) and 3(b). System scan speed can be greatly increased by scanning only a small number of positions. As in typical near-IR OCT systems, it is possible to fix the position of the reference mirror altogether, resulting in halving of the axial range of the scan, but greatly increased scan speed while simplifying the mechanics [12]. The large translation of the reference mirror was done

in this work to allow amplitude normalization, without which the reconstruction of the interferogram of Figs. 3(a) and 3(b) for the limited number of lasers would not have resulted in cancelation away from the zero path delay (e.g., larger side lobes). Additional speed increases can be obtained by improving the electronics to eliminate the lock-in amplifier.

In summary, we have demonstrated the tomography of a dielectric sample using a frequency agile QCL array source at terahertz frequencies. The electrically switched source suggests fast axial scan speeds. Improved axial resolution will result from a spectrally broader source. An increase in the number of elements in the source will allow greater scan depth and potentially a fixed reference mirror interferometer, greatly enhancing the scan speed and simplicity of the system.

References

1. D. M. Mittleman, S. Hunsche, L. Boivin, and M. C. Nuss, Opt. Lett. **22**, 904 (1997).
2. S. Zhong, Y. C. Shen, L. Ho, R. K. May, J. A. Zeitler, M. Evans, P. F. Taday, M. Pepper, T. Rades, and K. C. Gordon, Opt. Lasers Eng. **49**, 361 (2011).
3. T. Yasui, T. Yasuda, K.-I. Sawanaka, and T. Araki, Appl. Opt. **44**, 6849 (2005).
4. A. F. Fercher, C. K. Hitzenberger, G. Kamp, and S. Y. El-Zaiat, Opt. Commun. **117**, 43 (1995).
5. S. R. Chinn, E. A. Swanson, and J. G. Fujimoto, Opt. Lett. **22**, 340 (1997).
6. M. I. Amanti, M. Fischer, G. Scalari, M. Beck, and J. Faist, Nat. Photon. **3**, 586 (2009).
7. M. I. Amanti, G. Scalari, F. Castellano, M. Beck, and J. Faist, Opt. Express **18**, 6390 (2010).
8. B. G. Lee, M. A. Belkin, R. Audet, J. MacArthur, L. Diehl, C. Pflugl, F. Capasso, D. C. Oakley, D. Chapman, A. Napoleone, D. Bour, S. Corzine, G. Hofler, and J. Faist, Appl. Phys. Lett. **91**, 231101 (2007).
9. D. Burghoff, T.-Y. Kao, D. Ban, A. W. M. Lee, Q. Hu, and J. Reno, Appl. Phys. Lett. **98**, 061112 (2011).
10. W. H. Richardson, J. Opt. Soc. Am. **62**, 55 (1972).
11. S. Kumar, C. W. I. Chan, Q. Hu, and J. L. Reno, Nat. Phys. **7**, 166 (2011).
12. M. Choma, M. Sarunic, C. Yang, and J. Izatt, Opt. Express **11**, 2183 (2003).